F-x linear prediction filtering of seismic images

Mark P. Harrison

ABSTRACT

The f-x linear prediction filtering algorithm is reviewed and tested on several synthetic images. It is found that the f-x filter, when applied to noise-free synthetics, produces little or no attenuation of continuous layers, but does laterally smear sharp discontinuities. On noisy synthetic images, numerical measurements indicate that the f-x filter performs better at attenuating random noise than does the f-k filter. The f-x filter, however, produces greater lateral smearing of discontinuities than does the f-k filter. The residual noise after f-x filtering still appears fairly random, and the filter does not give rise to the same type of coherent "streaks" that a severe f-k filter is seen to create. In addition, the f-x filter is able to extract the signal without any guidance from the user, whereas an f-k dip reject filter must be manually selected, usually after inspection of a f-k spectrum plot. The f-x filter, however, is not able to discriminate between coherent noise with large dip and true events. Application of the f-x filter to an actual seismic image produces good results, and no attenuation of coherent signal is seen to occur.

INTRODUCTION

The signal-to-noise ratio for converted-wave stack images is often poor. This usually necessitates the application of some sort of image noise attenuation process, often in the form of f-k (frequency-wavenumber) or Karhunen-Loeve filtering (Jones and Levy, 1987). This paper looks at a different approach to signal-enhancement, f-x filtering, in which the seismic image is modelled as being composed of a number of linearly-coherent reflections. This justifies the use of a prediction method in the spatial direction of the f-x domain to optimally extract linear features and suppress random noise. This method was first proposed for seismic data by Canales (1984), and has since been elaborated upon by others (e.g. Gulunay, 1986). In the following sections the theory behind the method will be reviewed and a comparison of the relative performance of f-x and f-k filtering will be made.

THEORY

A seismic image represents a collection of zero-mean amplitude values that are functions of time **t** and horizontal location **x** (trace number). The image can usually be modelled at some scale (Canales, 1984) as being composed of a number N of continuous dipping reflectors, each with slope s_i, i.e.,

$$a(t,x) = \sum_{i=1}^{N} w_i * \delta(t-t_i) \quad , \qquad (1)$$

where $\mathbf{w}_i$ is the temporal wavelet associated with the i'th reflector, convolved with a Dirac spike located at time $\mathbf{t}_i$, and

$$t_i = \tau_i + s_i x.$$

τ_i is the intercept time at some reference x-location, and $\mathbf{s}_i$ is the slope of the reflector. Taking the fourier transform of equation 1 w.r.t time gives

$$a(\omega,x) = \sum_{i=1}^{N} W_i(\omega)\, e^{-j\omega(\tau_i+s_i x)}$$

where $\mathbf{W}_i(\omega)$ is the fourier transform of the wavelet $\mathbf{w}_i(\mathbf{t})$. This can be rewritten as

$$a(\omega,x) = \sum_{i=1}^{N} C_i(\omega)\, e^{-j\omega s_i x}$$

where $\mathbf{C}_i(\omega)$ is a complex function of ω only. This shows that each frequency, when viewed in the x-direction, is just a sum of weighed sinusoids of varying amplitudes and periods, implying that changes in a frequency component in the x-direction are predictable.

Given this predictable nature, it is possible to design a unit-distance prediction operator for each frequency that gives, in the least-squares sense, the most likely value for the next sample based on previous samples. This leads to the design of a complex least-squared-error prediction filter. The theory behind complex prediction filtering can be found in Treitel (1974), and is reviewed here. Letting the vector $\mathbf{f}$ be the prediction operator of length m+1 and the vector $\hat{\mathbf{a}}$ be the predicted values of $\mathbf{a}$, then, for each frequency, the filter equations can be written as

$$\begin{pmatrix} \hat{a}_0 \\ \hat{a}_1 \\ \vdots \\ \hat{a}_{m+n} \end{pmatrix} = \begin{pmatrix} a_0 & 0 & \cdots & 0 \\ a_1 & a_0 & & \vdots \\ \vdots & a_1 & & \\ & \vdots & & \\ a_n & & & 0 \\ 0 & a_n & & a_0 \\ & 0 & & \vdots \\ & & & \\ & & & a_{n-1} \\ 0 & 0 & \cdots & a_n \end{pmatrix} \begin{pmatrix} f_0 \\ f_1 \\ \vdots \\ f_m \end{pmatrix}$$

or

$$\hat{\mathbf{a}} = \mathbf{A}\mathbf{f},$$

where the a_i are samples in the x-direction and the ω subscript has been dropped. Defining the desired output as the vector $\mathbf{d}$, which, in this case, is just the sequence advanced by one sample, then the prediction error $\mathbf{e}$ will be

$$\begin{aligned} \mathbf{e} &= \mathbf{d} - \hat{\mathbf{a}} \\ &= \mathbf{d} - \mathbf{A}\mathbf{f}, \end{aligned}$$

and the error energy will be

$$\mathbf{I} = \mathbf{e}^H\mathbf{e}$$

where $\mathbf{e}^H$ is the transposed complex conjugate of $\mathbf{e}$. The error energy becomes

$$\mathbf{I} = (\mathbf{d}-\mathbf{Af})^{H}(\mathbf{d}-\mathbf{Af})$$
$$= \mathbf{d}^{H}\mathbf{d} - \mathbf{f}^{H}\mathbf{A}^{H}\mathbf{d} - \mathbf{d}^{H}\mathbf{Af} + \mathbf{f}^{H}\mathbf{A}^{H}\mathbf{Af}.$$

The error energy can be minimized by taking the derivative w.r.t. the filter vector **f** and setting to zero, i.e.,

$$\frac{\partial \mathbf{I}}{\partial \mathbf{f}} = -\mathbf{d}^{H}\mathbf{A} + \mathbf{f}^{H}\mathbf{A}^{H}\mathbf{A} = 0,$$

or

$$\mathbf{f}^{H}\mathbf{A}^{H}\mathbf{A} = \mathbf{d}^{H}\mathbf{A}. \tag{2}$$

Taking the complex conjugate and transposing, this becomes

$$\mathbf{A}^{H}\mathbf{Af} = \mathbf{A}^{H}\mathbf{d}.$$

Defining the complex autocorrelation matrix **R** as

$$\mathbf{R} = \mathbf{A}^{H}\mathbf{A}$$

and the complex cross-correlation matrix **g** as

$$\mathbf{g} = \mathbf{A}^{H}\mathbf{d},$$

then equation 2 becomes

$$\mathbf{Rf} = \mathbf{g}. \tag{3}$$

These are the complex-valued normal equations that must be solved for the complex filter **f**. The complex matrix **R** can be written in the form

$$\mathbf{R} = \mathbf{P} + j\mathbf{Q}$$

where **P** is real and symmetric, and **Q** is real and skew-symmetric, i.e.,

$$\mathbf{Q}^{t} = -\mathbf{Q}$$

where $\mathbf{Q}^{t}$ is the transpose of **Q**. Treitel (1974) shows that by breaking equation 3 into it's real and imaginary parts, it can be rewritten as a second matrix equation;

$$\begin{pmatrix} \mathbf{P} & -\mathbf{Q} \\ \mathbf{Q} & \mathbf{P} \end{pmatrix} \begin{pmatrix} \mathbf{f}^{Re} \\ \mathbf{f}^{Im} \end{pmatrix} = \begin{pmatrix} \mathbf{g}^{Re} \\ \mathbf{g}^{Im} \end{pmatrix} \tag{4}$$

where **Re** and **Im** designate the real and imaginary parts of a function. This real-valued matrix equation can be solved to give the filter coefficients **f**. For the process being studied here, the **g** vector is just the first sub-diagonal column of the **R** matrix, plus one additional lag. The left matrix in equation 4 is block-Toeplitz (Treitel, 1974), and can be inverted using a Levinson-like recursion given by Robinson (1967).

Solving Equation 4 will result in the prediction operator to be applied in the +x direction. Prediction can also be done in the -x direction, giving left and right prediction operators. For prediction in the -x direction, reversing the sample order and going through a similar derivation leads to the folowing;

$$\mathbf{R}^*\mathbf{f}_- = \mathbf{g}^*.$$

Taking the complex conjugate, this becomes

$$\mathbf{R}\mathbf{f}_-^* = \mathbf{g},$$

which shows that the -x prediction operator is just the complex-conjugate of the +x prediction operator. A single filter, incorporating both +x and -x prediction, is then given by

$$\left(\frac{f_m^*}{2}, \frac{f_{m-1}^*}{2}, \ldots, \frac{f_0^*}{2}, 0, \frac{f_0}{2}, \ldots, \frac{f_{m-1}}{2}, \frac{f_m}{2}\right)^t \tag{5}$$

where the coefficients have been divided by 2 to give proper normalization. The computation and application of this filter to the complex series $\mathbf{a}(\mathbf{x})$ for each frequency then gives the prediction-filtered set $\hat{\mathbf{a}}(\omega,\mathbf{x})$, which is then inverse-transformed to give the f-x filtered output.

A difference image can be constructed by taking the point-by-point difference between the input image and the filtered image;

$$d(t,x) = a(t,x) - \hat{a}(t,x) \tag{6}$$

and is often useful in evaluating the performance of the filter.

METHOD AND RESULTS

The flow followed in implementing the f-x algorithm is outlined in Figure 1. To illustrate the method, a simple synthetic image (Figure 2) was created with only a single linear event. This event was generated by convolving a 8-75 hz bandpass filter operator with a spike placed at the time position appropriate for each trace. The input image is first fourier-transformed in time to give a complex frequency series at each trace (x) location. These traces are then reordered to give for each frequency a sequence of complex samples, one sample from each of the transformed traces in the x-direction. The complex autocorrelation for each of the frequency sequences is then generated, and the first m+1 lags are used to generate the prediction operator. For the examples given in this paper, 7 lags were used, giving a total operator length of 15 samples (7 in each direction). The resulting operator is then convolved with the x-ordered sequence for that frequency, and the process is repeated until all frequencies in the transformed data set have been done. These filtered sequences are reordered back into their respective x-trace positions, and the inverse fourier transform is applied, giving the filtered result shown in Figure 3. To assess the result of applying the filter, the sample-by-sample differences between the input image and the filtered output image were computed using equation 6, and are plotted in Figure 4. As expected for this simple example, the prediction worked very well, and Figure 4 shows that there is no visible difference between the input and output images.

To assess the filter's ability to suppress random noise, the synthetic image of Figure 2 was corrupted with random noise with a bandwidth of 6-120 hz, which approximates the bandwidth of a seismic field recording system. The variance of the noise was made equal to the variance of the 200 ms bandpass wavelet used to construct the

original synthetic. The resulting image is shown in Figure 5, and is seen to have a severe noise level, close to the upper limit of that normally found on a seismic image. In order to roughly assess the filter's noise-suppression capabilities, a portion of the image, outlined in Figure 5, was selected over which the noise variance levels before and after filtering were computed. In this case, it was found that the filter attenuated the dipping reflector by about 35%. To account for this, the filtered image was scaled by a constant factor to bring the amplitudes of the dipping event closer to it's original level (Figure 6), and a difference image was computed (Figure 7). From the difference image, it is seen that a substantial amount of noise has been rejected. Measurements within the control portion of the image indicate a reduction in the noise variance of 16.6 db.

An f-k filter was also applied to the noisy image for comparison, giving the result shown in Figure 8. A comparison of the f-k filtered image and the f-x filtered image (Figure 6) shows that both have done a comparable job of attenuating the noise. The noise left by the f-k filter appears very coherent, whereas the noise left by the f-x is more random and lower frequency. Measurements within the control portion indicate a reduction in the noise variance of 14.8 db, compared to 16.6 db for the f-x filter.

A more complicated synthetic was constructed, having reflectors with discontinuities and conflicting dips, as well as two large-amplitude noise glitches. Random noise identical in amplitude and frequency to that used in the previous example was added, giving the results shown in Figure 9. A control portion for attenuation comparison was also selected for this image, and is outlined in the figure. The result of f-x filtering the image is shown in Figure 10. The two large-amplitude glitches are largely removed, and there is little smearing of the glitches into adjacent traces. The discontinuity on the top flat horizon is seen to have been spread horizontally over a distance of seven traces (the width of the prediction filter). The difference image, which is not shown here, shows about a 15% loss of amplitude on the two steepest events, relative to the other reflectors. Measurements made within the control portion give a reduction in noise variance of 8.4 db.

An f-k filter was also applied to the image of Figure 9, giving the result shown in Figure 11. Comparison of the f-x filtered image (Figure 10) and the f-k filtered image (Figure 11) indicates that both methods have achieved roughly the same amount of noise attenuation, with the noise remaining in the f-k filtered image again appearing higher frequency and less random than in the f-x filtered image. The f-k filter is seen to produce less lateral tapering of the discontinuity on the top flat event than does the f-x filter. Measurements made within the control portion indicate a 4.7 db reduction in the noise variance, compared to 8.4 db for the f-x filter.

Plotted in Figure 12 is an f-k power spectrum of the noisy input image, which shows the noise to be evenly distributed over the entire f-k spectrum. The most steeply-dipping event is seen to alias at frequencies greater than about 65 hz. An f-k power plot of the f-k filtered section of Figure 11 is displayed in Figure 14, and shows that the noise has been removed from the spectrum everywhere except within the wedge enclosing the dipping events. The filter has also removed the aliased frequencies of the most steeply-dipping event, which produces a change in waveform shape for that event. Figure 13 is an f-k power plot of the f-x filtered image of Figure 10, from which it is seen that the noise has been uniformly attenuated throughout the spectrum, including within and beneath the signal band where f-k filtering has had no effect.

As a final example, the f-x filter was run on the radial-component section of line FS90-1 in the Springbank, Alberta area (Lawton and Harrison, 1990) The original and f-x filtered sections are displayed in Figures 15 and 16 respectively. For comparison, an f-k filter was also applied, giving the section shown in Figure 17. The f-x filter is seen to give

better overall continuity than does the f-k filter. The very high-dip noise trains have not been attenuated by the f-x filter, but have been removed by the f-k filter.

DISCUSSION

The main parameters that the user of an f-x filter has to decide upon are the length of the prediction filter and the size of the window in which it is designed. In the complicated synthetic, a longer operator and/or a smaller window size probably would have given better preservation of the most steeply-dipping events, but no work has been done to confirm this. The choice of seven lags for the operator length appears to work well in the examples presented here, but it is possible that a longer operator might have produced better results. A major constraint on the length of the filter operator, however, is the computational cost of having to design a filter for each individual frequency. In order that the method be practical, it is desirable to keep the number of lags used as small as possible.

An area for further testing of the f-x filter is in cases where events are curved, and have amplitude variations. If these events are altered or discarded by the filter, then the method may have limited use in areas of large sub-surface structure. Also, Gulunay (1986) gives a proof that f-x filtering does not work correctly if events with conflicting dips are present, as could occur in structured areas. From the synthetic images shown here, as well as other tests, it appears, however, that the filter still performs well when this happens.

From the synthetic examples, it is seen that the f-x filter is better at attenuating random noise than is the f-k filter. The residual noise after f-x filtering still appears fairly random, and it does not give rise to the same type of coherent "streaks" that a severe f-k filter is known to produce. In addition, the f-x filter is able to extract the signal without any guidance from the user, whereas an f-k dip reject filter must be manually selected, usually after inspection of an f-k spectrum plot. The f-x filter therefore appears to have some important advantages over the f-k filtering method. It is seen from Figure 16 that the f-x filter is not able to distinguish coherent linear noise from true reflections, which can be a disadvantage. It is possible that better results could be obtained in some cases by using both an f-x filter to remove random noise, and a mild f-x to remove high-dip coherent noise.

CONCLUSIONS

The f-x linear prediction filter was reviewed and tested on several synthetic images. It was found that the filter, when applied to noise-free synthetics, produces little or no attenuation of continuous layers, but does laterally smear sharp discontinuities. On noisy synthetic images, numerical measurements indicate the f-x filter performs better at attenuating random noise than the f-k filter. The residual noise after f-x filtering still appears fairly random, and the filter does not give rise to the same type of coherent "streaks" that a severe f-k filter was seen to produce. In addition, the f-x filter is able to extract the signal without any guidance from the user, whereas an f-k dip reject filter must be manually selected, usually after inspection of a f-k spectrum plot. The f-x filter is not able to attenuate coherent dipping noise, which appears to the algorithm as valid signal. Application of the f-x filter to an actual seismic image produced results which compared favorably to those obtained by f-k filtering.

REFERENCES

Canales, L.L., 1984, Random noise attenuation: Presented at the 54th Ann. Mtg., Soc. Explor. Geoph.

Gulunay, N., 1986, FXDECON and complex Wiener prediction filter: Presented at the 56th Ann. Mtg., Soc. Explor. Geoph.

Jones, I.F., and Levy, S., 1987, Signal-to-noise ratio enhancement in multi-channel seismic data via the Karhunen-Loeve transform: Geophysical Prospecting, v. 35, 12-32.

Lawton, D., and Harrison, M., 1990, A two-component reflection seismic survey, Springbank, Alberta: in this volume.

Robinson, E.A., 1967, Multichannel time series analysis with digital computer programs: San Francisco, Holden-Day.

Treitel, S., 1974, The complex wiener filter: Geophysics, v. 39, 169-173.

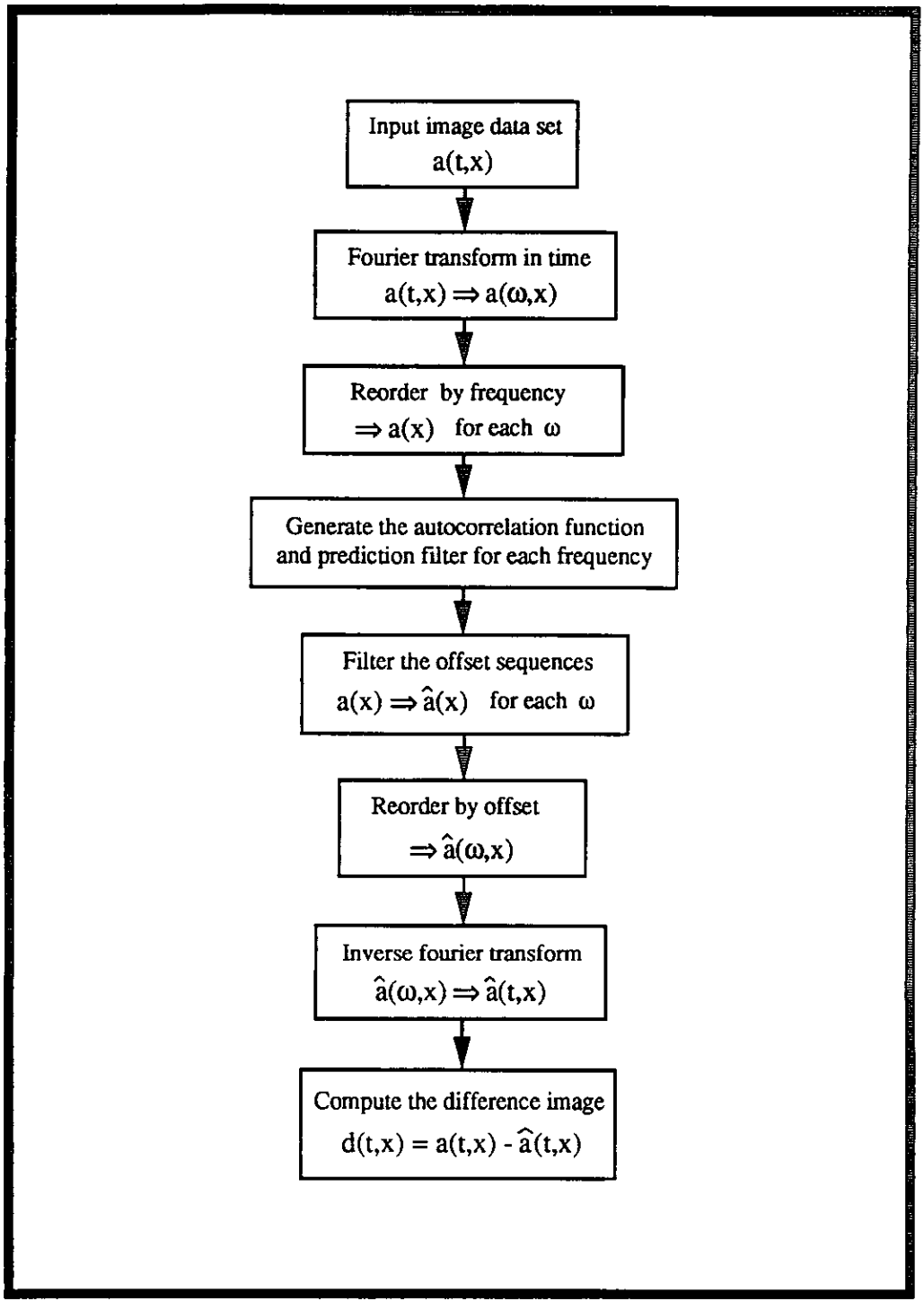

Fig. 1. Process flowchart for the f-x filtering algorithm.

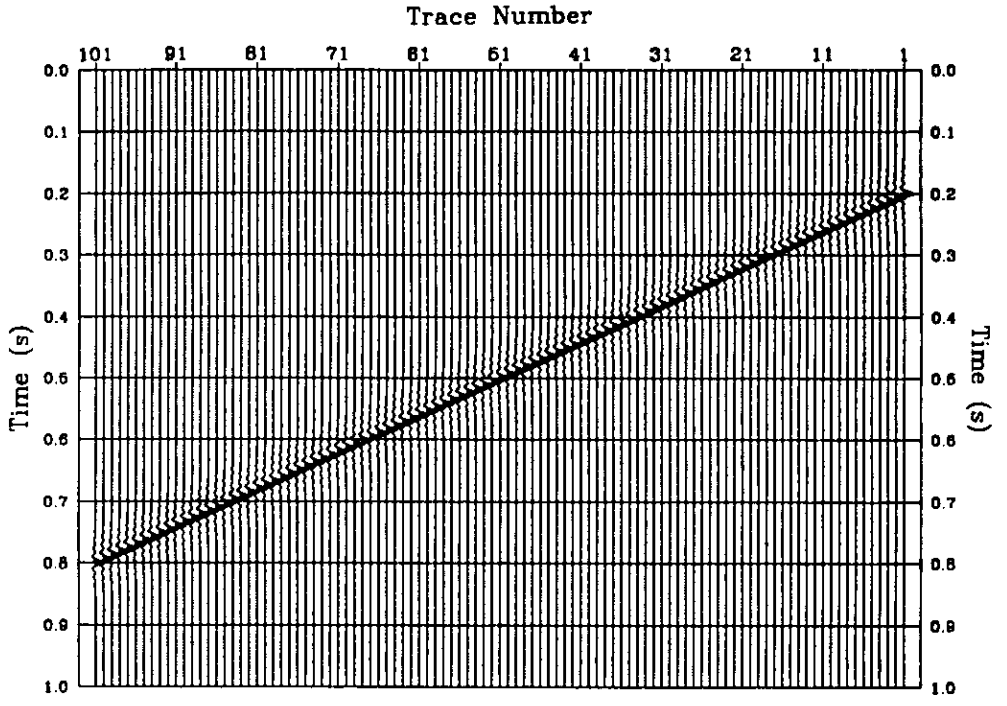

Fig. 2. A simple model with a single linear reflection. The wavelet bandwidth used is 8-75 hz.

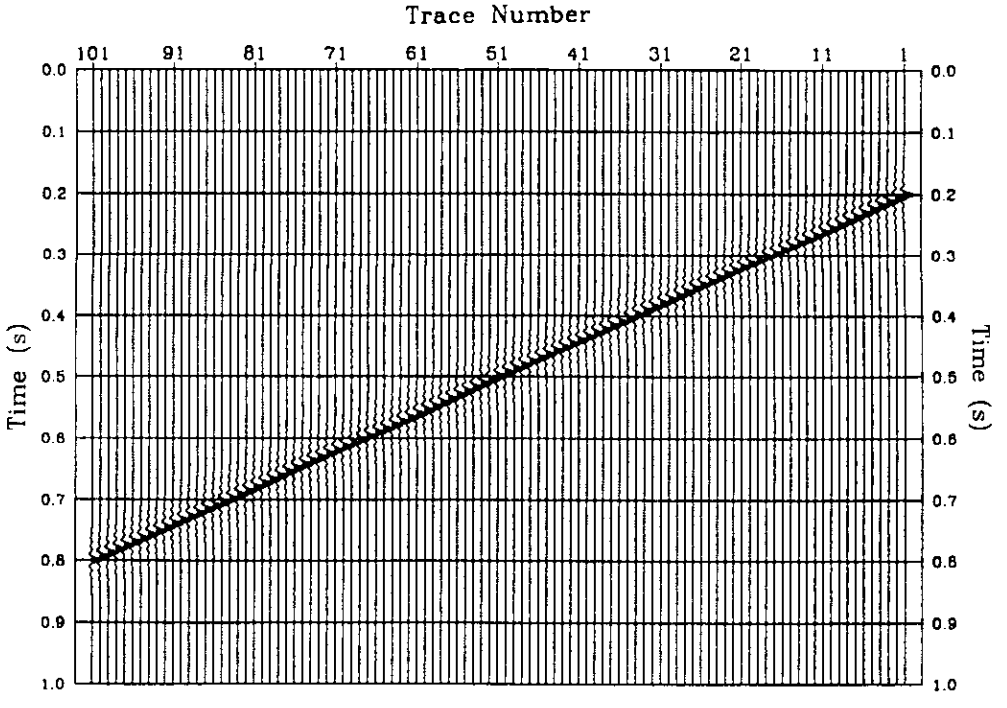

Fig. 3. The f-x filtered version of the image in Figure 2.

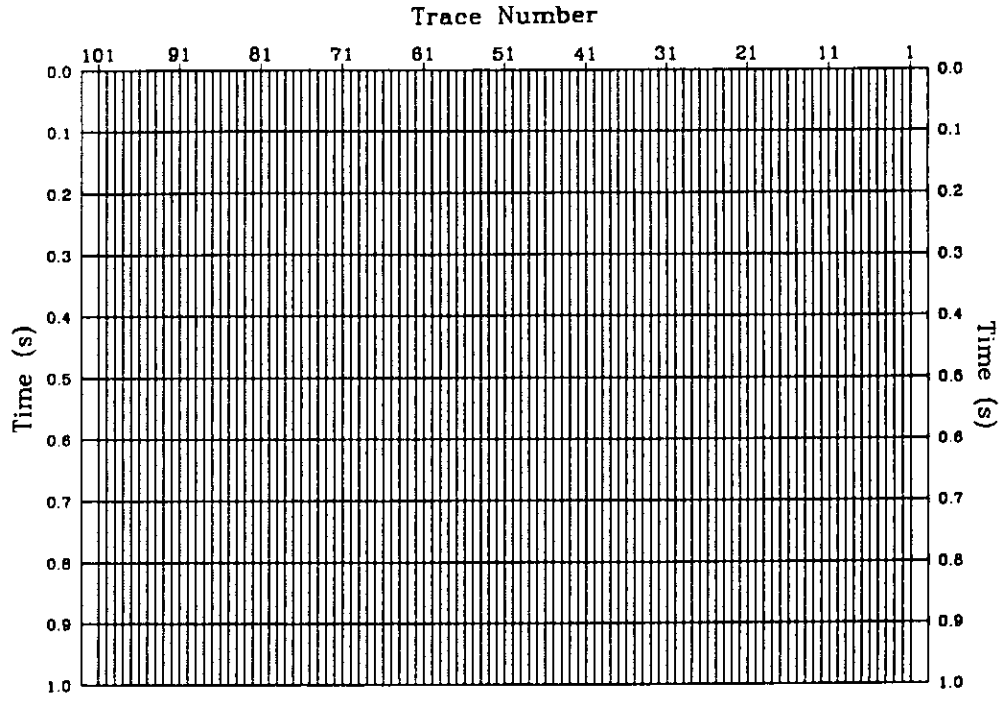

Fig. 4. The difference between the input image (Figure 2) and the f-x filtered image (Figure 3).

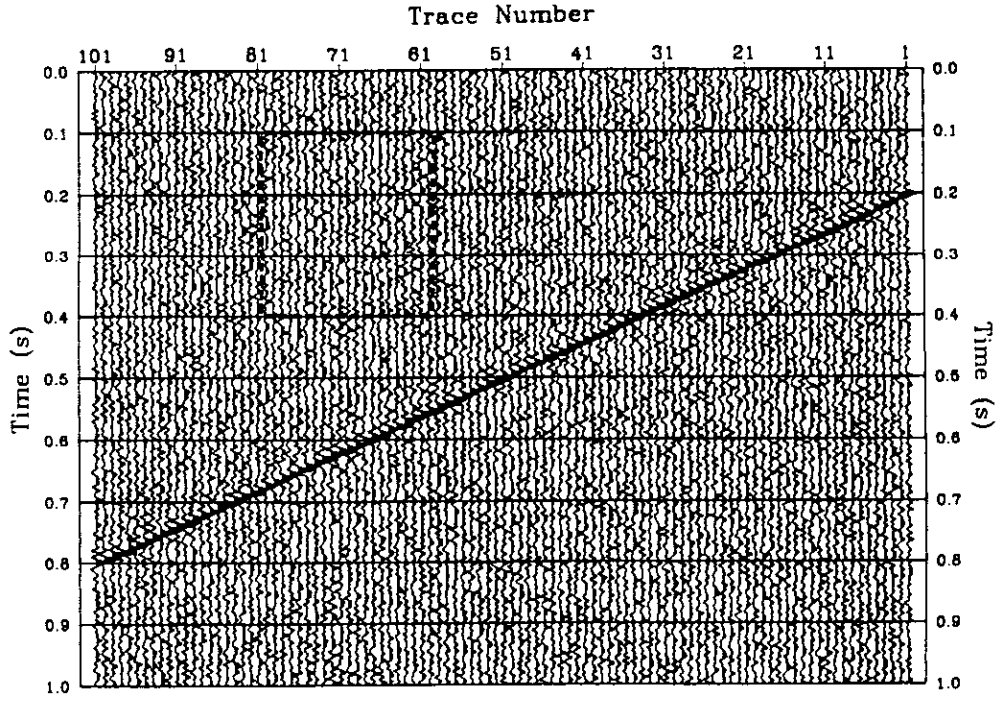

Fig. 5. Band-limited random noise added to the synthetic image in Figure 2. The box indicates the area over which noise variances were calculated.

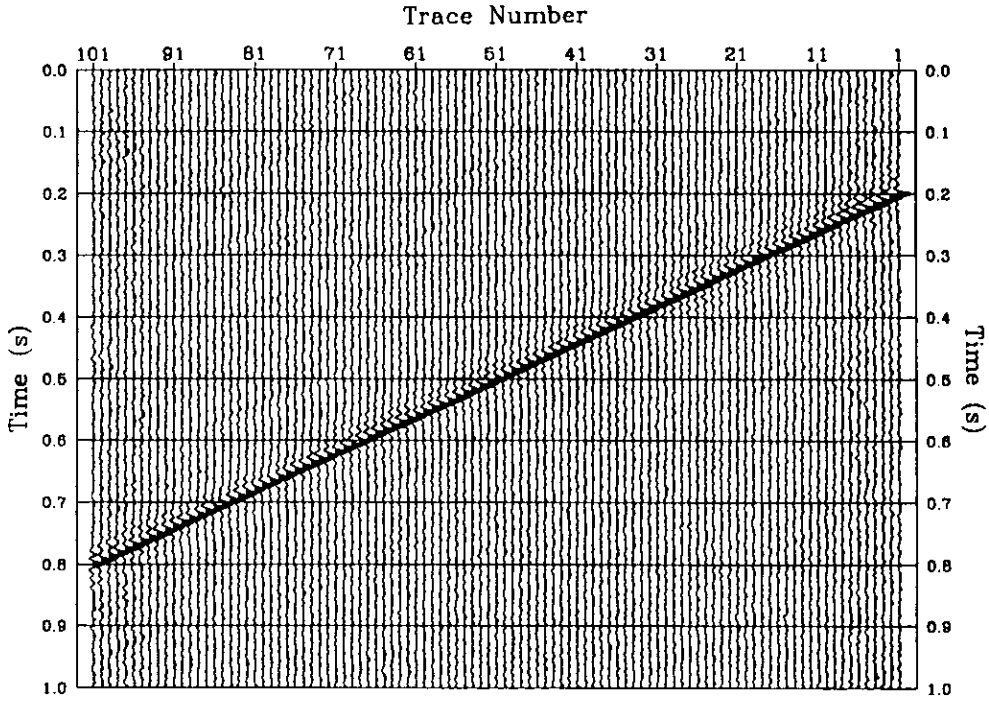

Fig. 6. The f-x filtered version of the image in Figure 5.

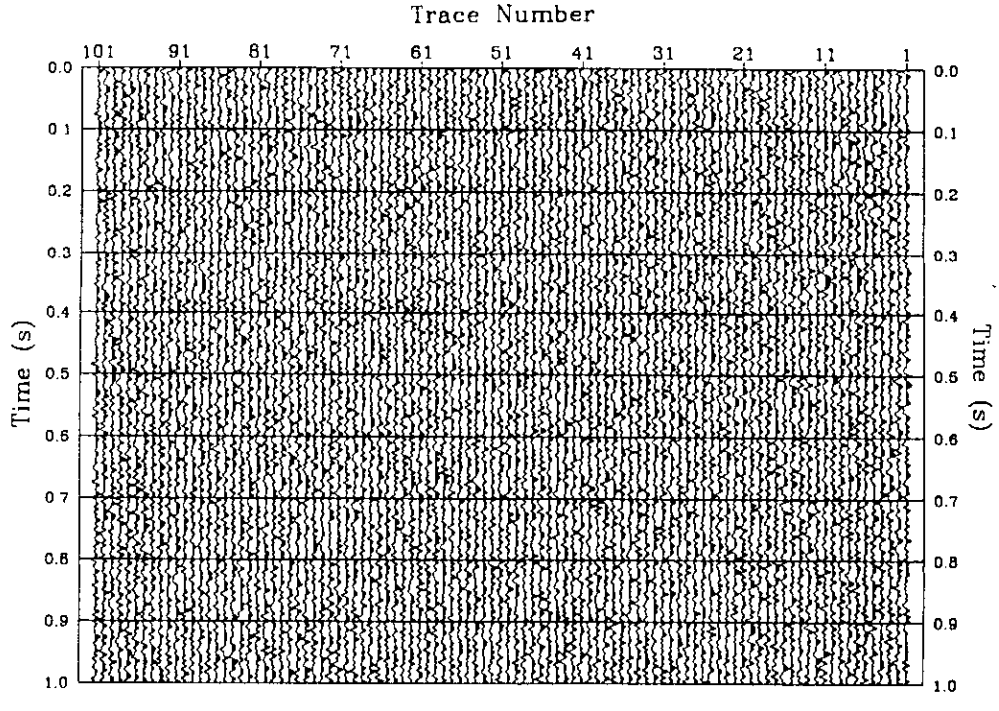

Fig. 7. The difference between the input image (Figure 5) and the f-x filtered image (Figure 6).

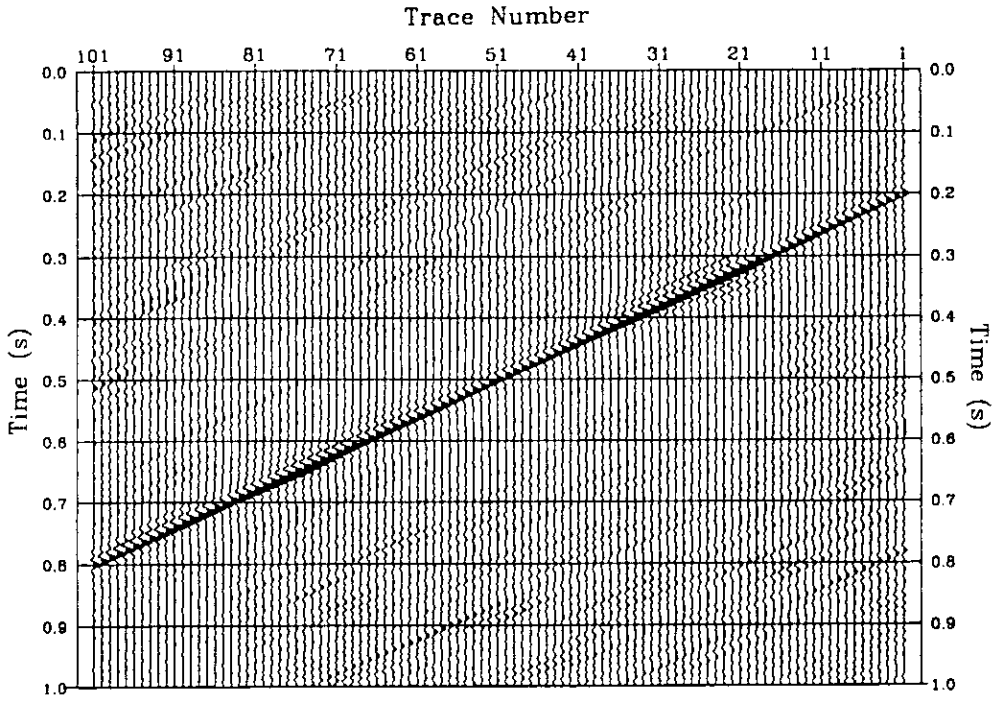

Fig. 8. The result of applying an f-k filter to the noisy image of Figure 5.

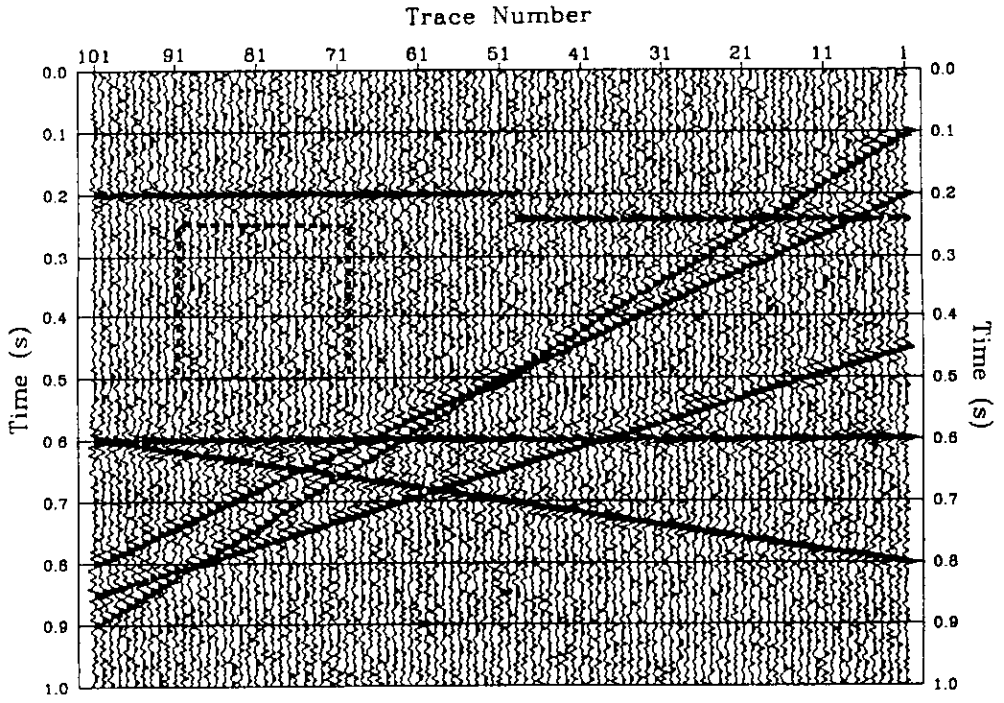

Fig. 9. A more complicated synthetic image with various dipping reflections, a discontinuity, a pair of noise glitches, and band-limited noise. The box indicates the area over which noise variances were calculated.

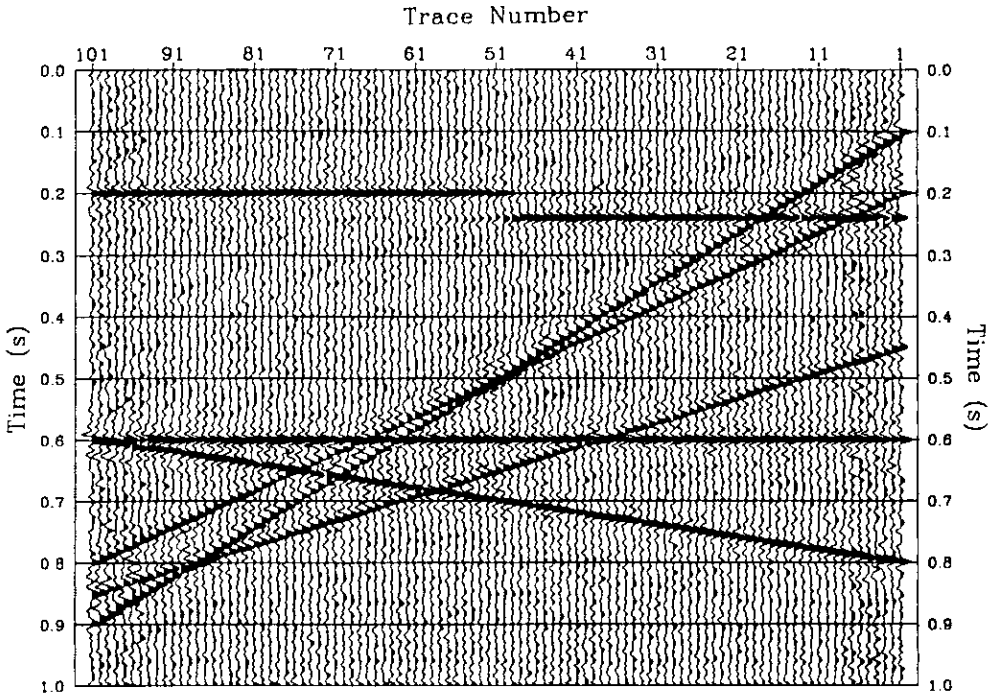

Fig. 10. The f-x filtered version of the image in Figure 9.

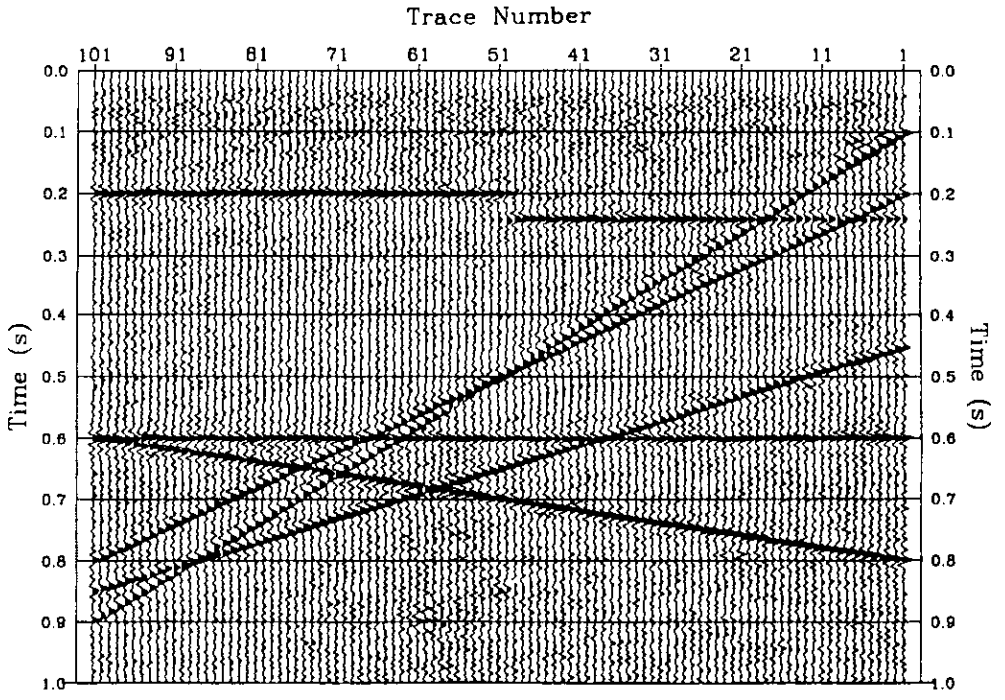

Fig. 11. The f-k filtered version of the image in Figure 9.

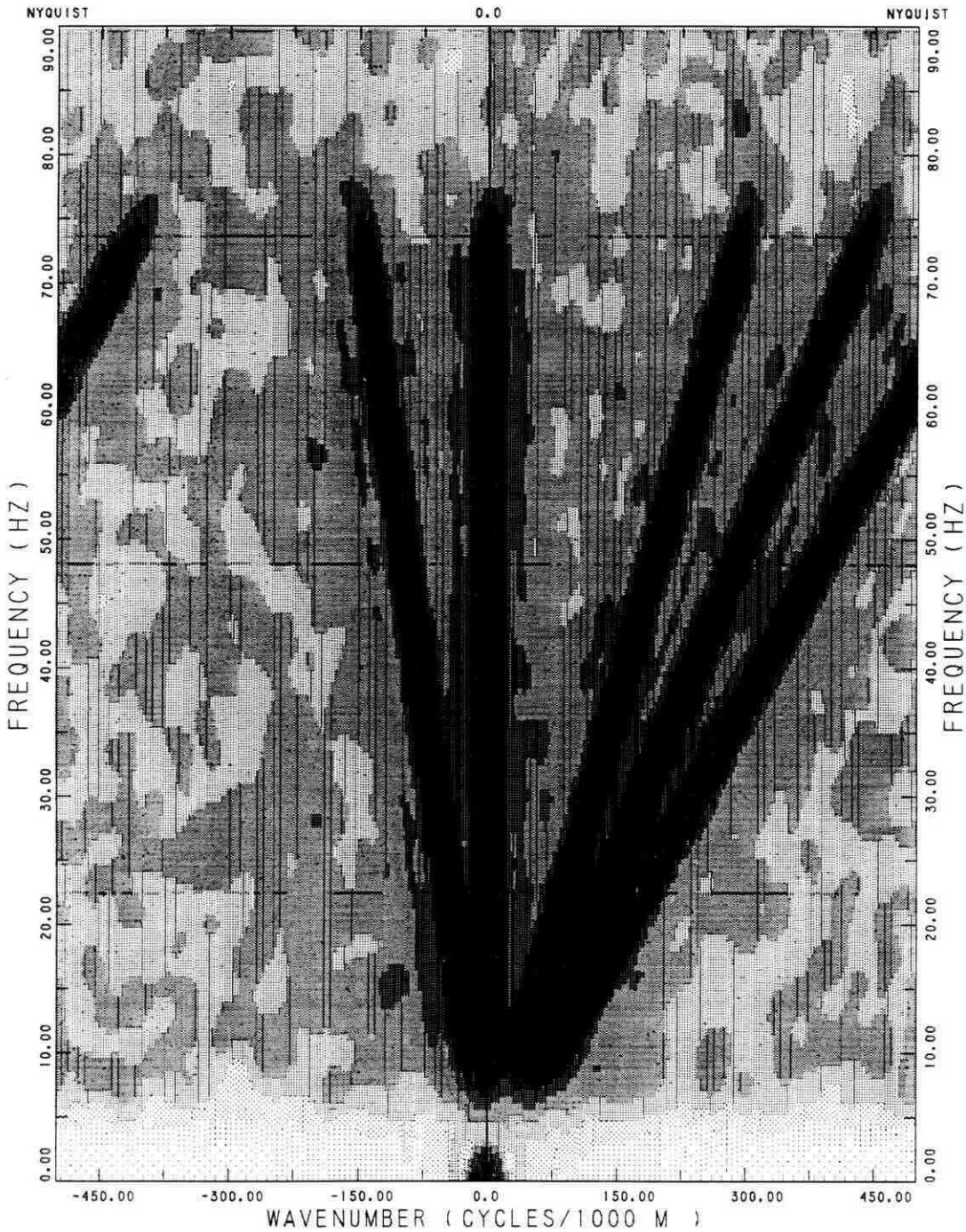

Fig. 12. An f-k spectrum power plot of the input image shown in Figure 9.

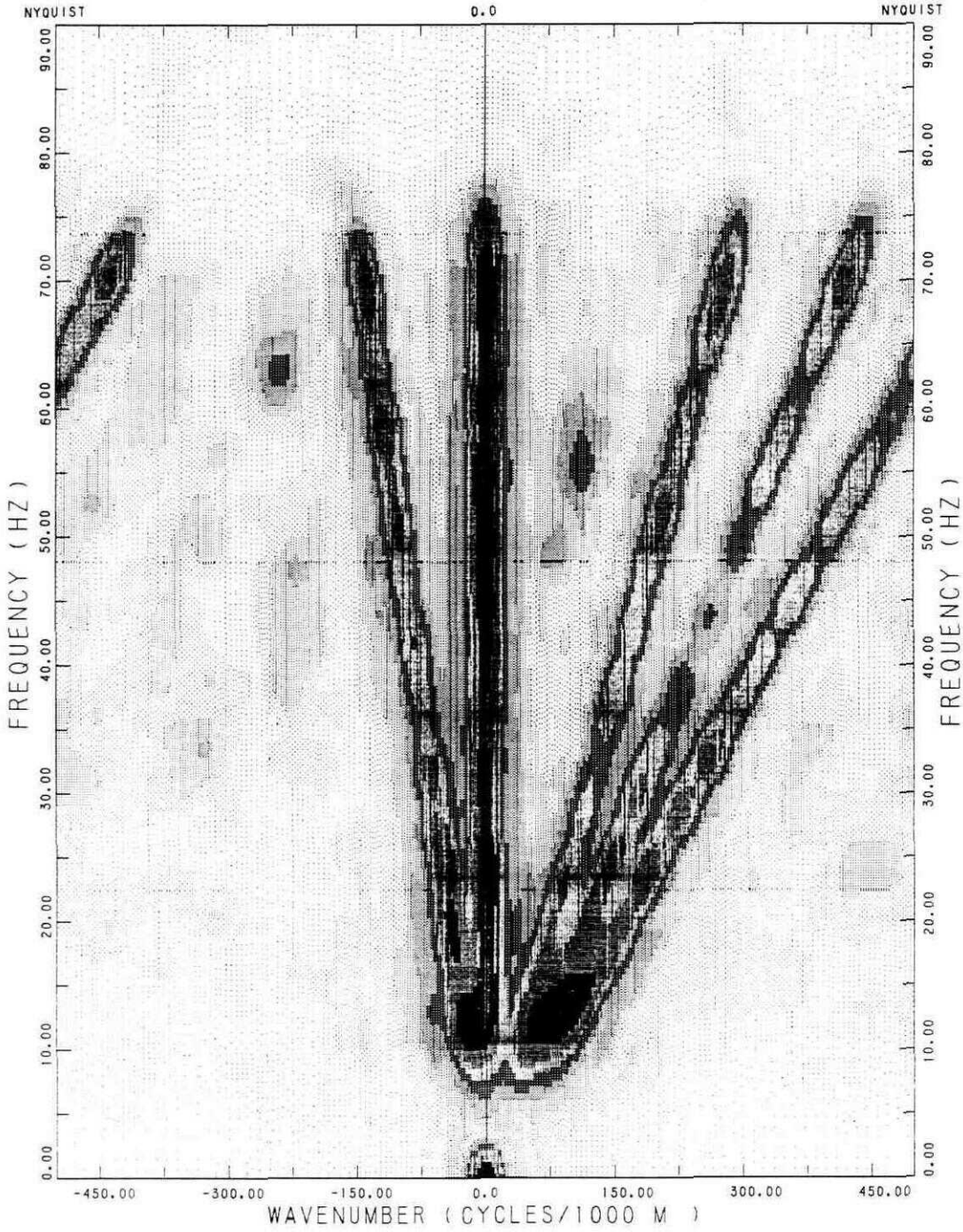

Fig. 13. An f-k spectrum power plot of the f-x filtered image shown in Figure 10.

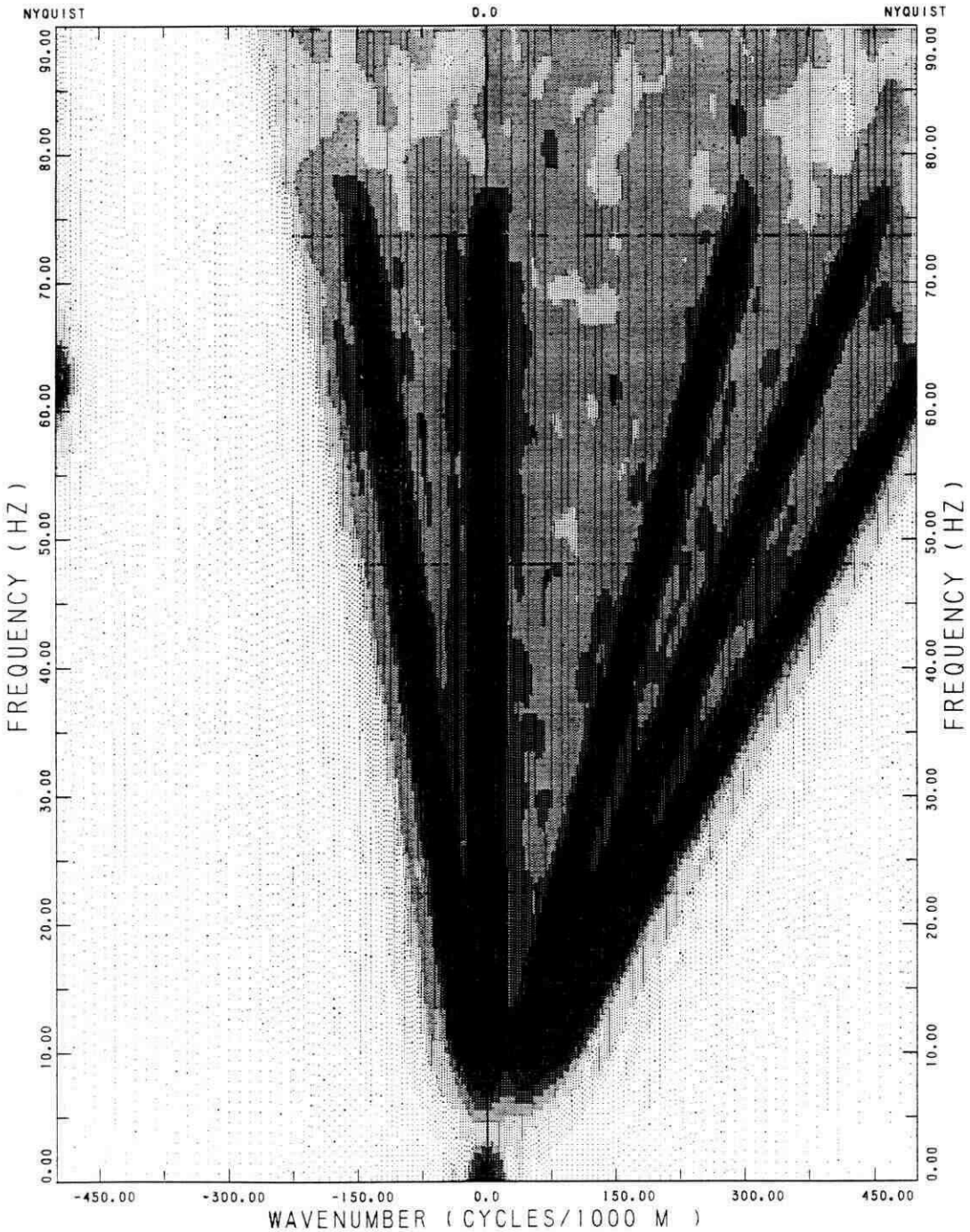

Fig. 14. An f-k spectrum power plot of the f-k filtered image shown in Figure 11.

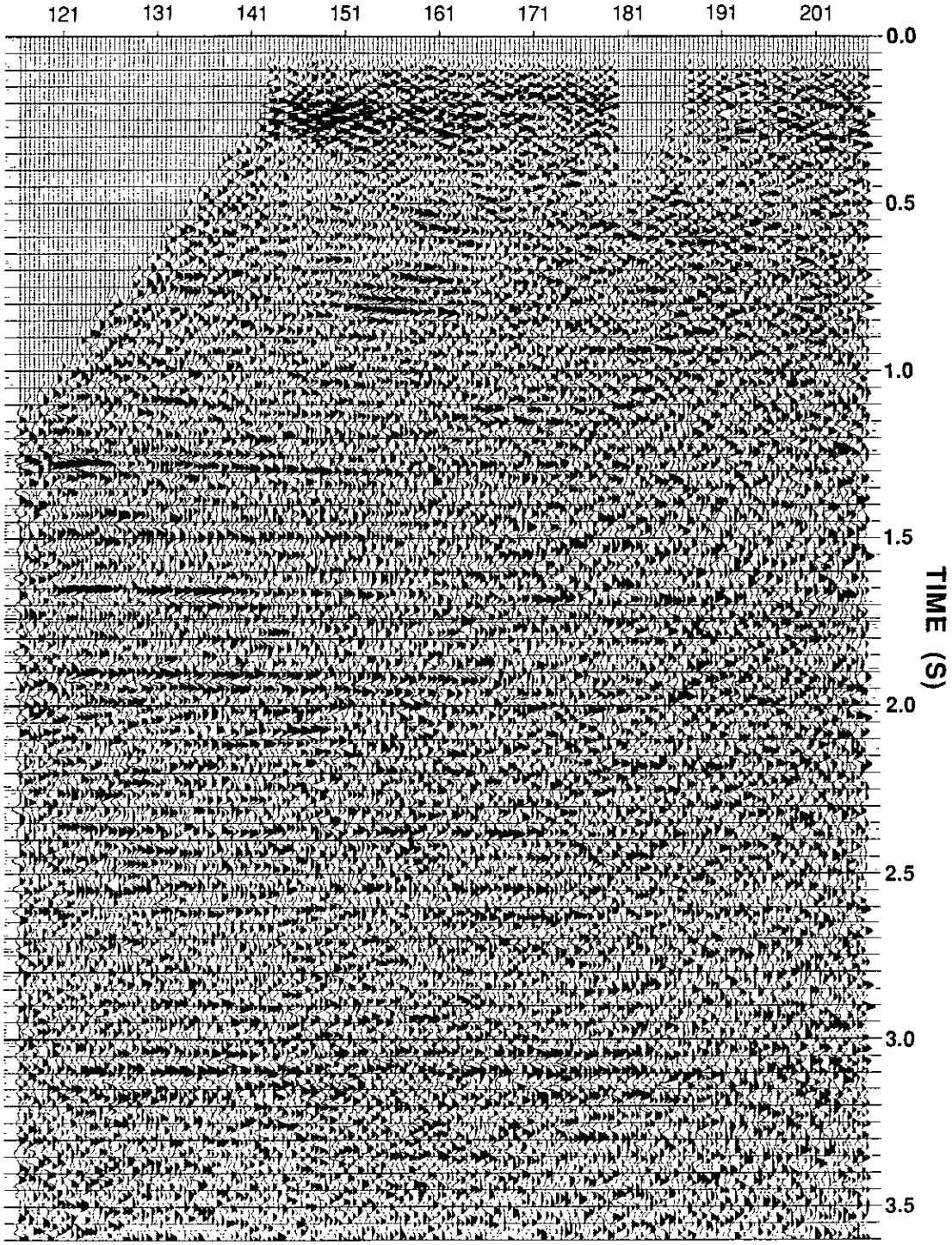

Fig. 15. A converted-wave section.

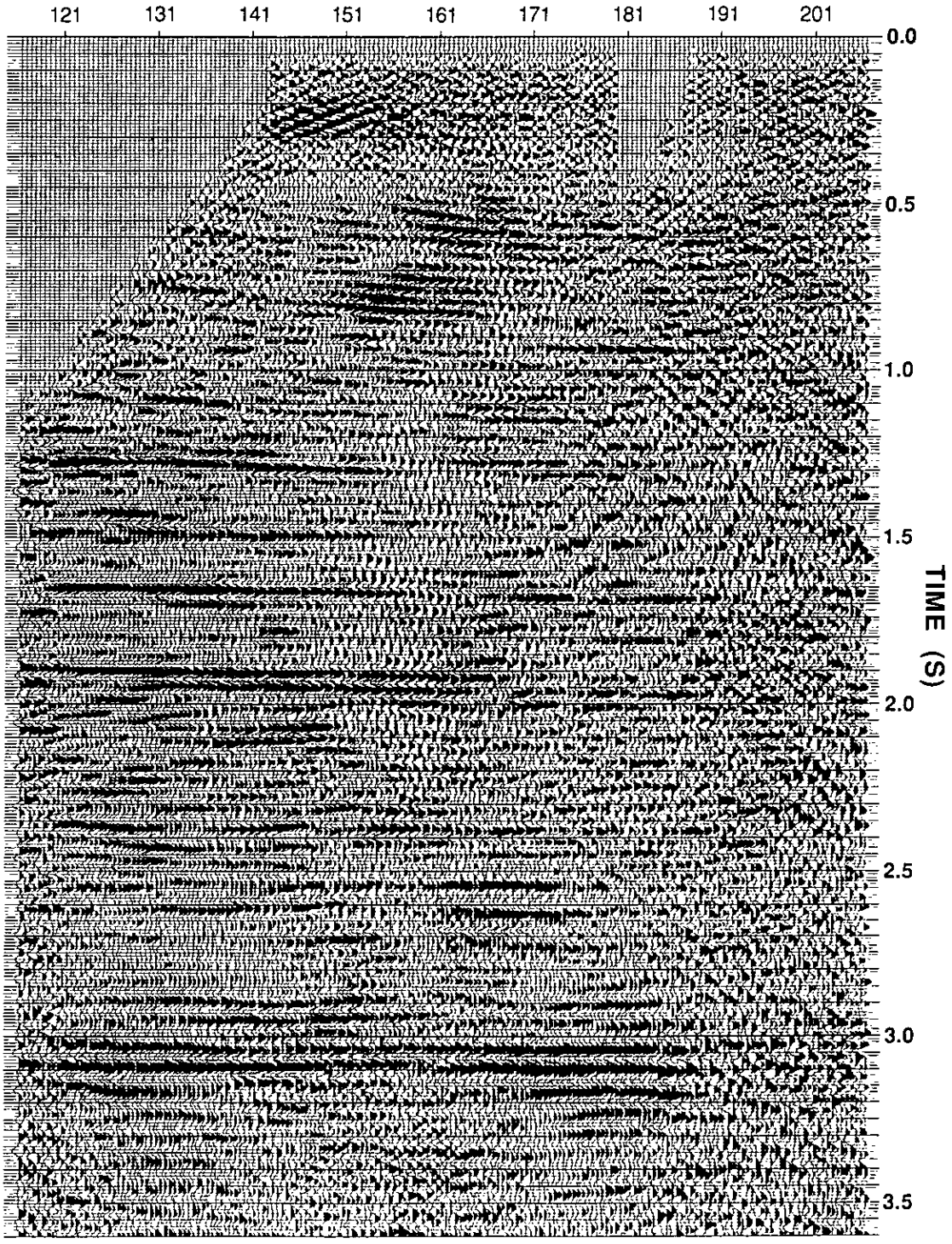

Fig. 16. The f-x filtered version of the section shown in Figure 15.

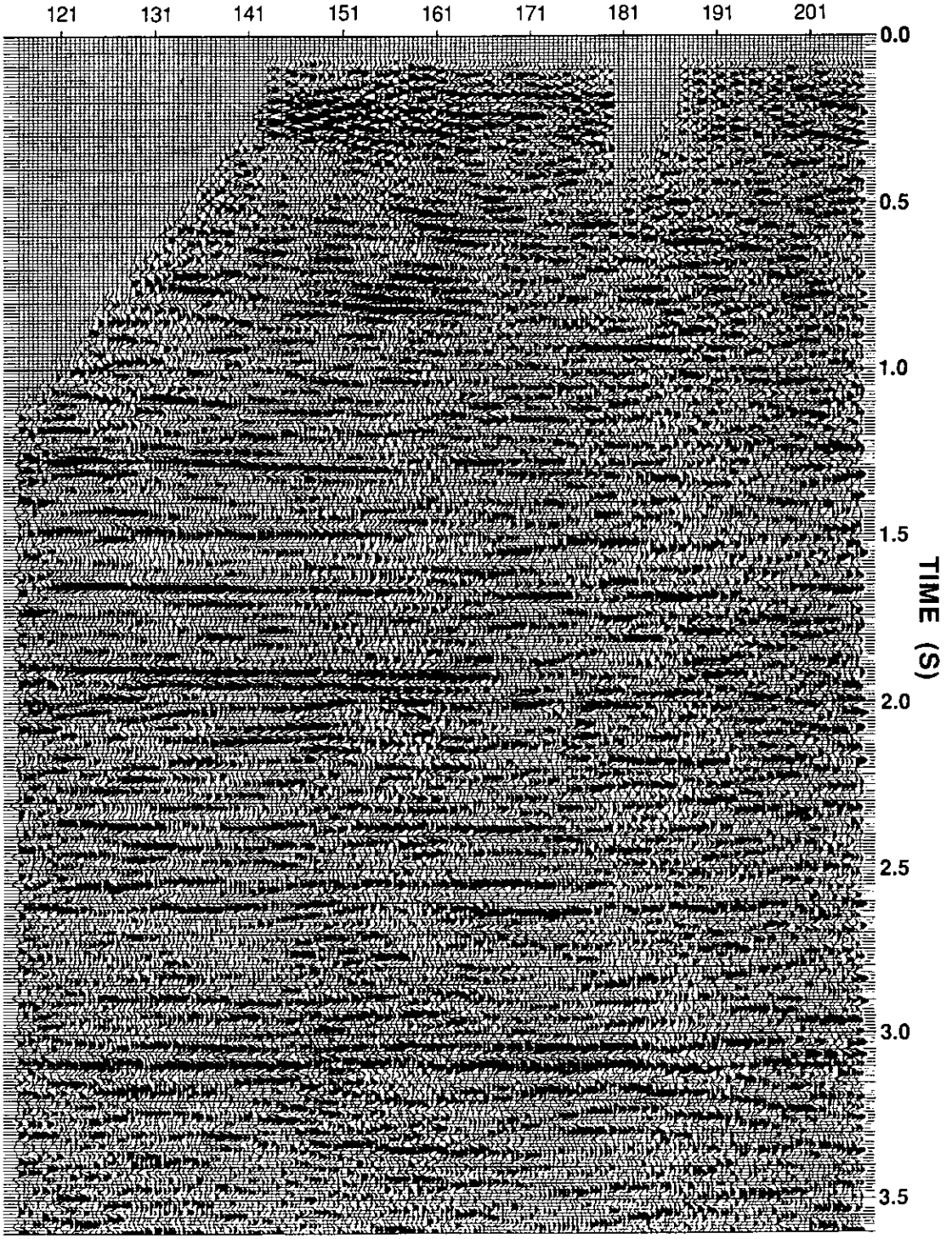

Fig. 17. The f-k filtered version of the section shown in Figure 15.